



# Cosmological constraints on mass-varying dark matter

Amlan Chakraborty <sup>1,\*</sup> Anirban Das <sup>2,†</sup> Subinoy Das<sup>1,‡</sup> and Shiv K. Sethi<sup>3,§</sup>

<sup>1</sup>*Indian Institute of Astrophysics, Bengaluru, Karnataka 560034, India*

<sup>2</sup>*Center for Theoretical Physics, Department of Physics and Astronomy,  
Seoul National University, Seoul 08826, South Korea*

<sup>3</sup>*Raman Research Institute, C. V. Raman Avenue, Sadashivanagar, Bengaluru 560080, India*

Light mass warm dark matter is an interesting and viable alternative to the cold dark matter paradigm. An intriguing variation of this scenario is the mass-varying dark matter model where the dark matter mass varies with time during its cosmic history. This is realized in multiple particle physics models. In this work, we study the cosmological constraints on such a model where the dark matter mass transitions from zero to a finite value in the early Universe. In this model, the matter power spectrum exhibits power suppression below a scale that depends on the epoch of transition, and the angular power spectrum of the cosmic microwave background show a distinctive phase shift. We use the latest cosmic microwave background and the weak lensing data to place lower limit on the transition redshift and ease the  $S_8$  tension, unlike the warm dark matter model. This analysis also facilitates a marginal detection of the dark matter (DM) mass. Our findings reveal that while Planck data alone reduces the  $S_8$  tension to approximately  $2\sigma$ , it does not sufficiently constrain the DM mass. However, when combined with the  $S_8$  measurement from KIDS1000+BOSS+2dfLenS, the tension significantly decreases to roughly  $1.3\sigma$ , and we observe the detection of a DM mass at  $41.7^{+7.81}_{-27.5}$  eV. Further analysis incorporating a combined data set from ACT and weak lensing results in an even more pronounced reduction in the tension to approximately  $0.4\sigma$ , alongside a higher detected mass of  $51.2^{+16}_{-33.5}$  eV. We also find a better fit to the combined data compared to the  $\Lambda$ CDM model.

## I. INTRODUCTION

Planck observations of the Cosmic Microwave Background (CMB) tells us that dark matter (DM) forms the dominant share of all matter in the Universe [1]. The most successful theory to explain the observations at different scales, ranging from galaxies and galaxy clusters to the horizon is the  $\Lambda$ CDM model, which includes a cosmological constant  $\Lambda$  and cold collisionless dark matter (CDM). All of these observations are however based on the gravitational effects of DM on the visible Universe, and hence, its exact particle nature remains elusive till date.

Numerous laboratory and space-based experiments have been conducted over the past few decades to shed light on the elusive particle nature of DM. However, despite these efforts, no conclusive evidence of non-gravitational interactions with standard model particles has been found yet. In particular, the non-detection of weakly interacting massive particles (WIMPs), considered the most promising candidate for DM over the last two decades, has raised concerns [2]. This has resulted in a wider search program in the DM model space. It also underscores the importance of a more careful study of the gravitational signatures of DM in cosmology. Additionally, small-scale problems related to the structure formation of the universe, such as the missing satellite

problem, Core vs cusp problem, and too-big-to-fail problem, have further motivated the exploration of beyond-cold dark matter (CDM) models. While some of these issues have been addressed through baryonic feedback, it is still worthwhile to investigate alternative scenarios beyond CDM for cosmological purposes.

Warm dark matter (WDM) and mixed dark matter, which is a combination of hot dark matter (HDM) and WDM or CDM, have been proposed as alternatives to CDM to solve small-scale problems due to their free-streaming properties, which result in less structure formation at small scales [3–6]. It reduces the number of satellite galaxies in halos and suppresses the halo mass function. However, in addition to these small-scale problems, the standard  $\Lambda$ CDM model has been challenged by cosmological tensions such as the Hubble tension and the  $S_8$  tension [7].

The clumpiness of the matter distribution in our Universe is parameterized by  $S_8 = \sigma_8(\Omega_m/0.3)^{0.5}$ , where  $\sigma_8$  is the root mean square of matter fluctuations on an  $8h^{-1}$  Mpc scale, and  $\Omega_m$  is the total matter abundance. In  $\Lambda$ CDM, Planck observation yields  $S_8 = 0.832 \pm 0.013$  [1]. The observation of weak lensing of galaxies from the CFHTLenS collaboration initially pointed to a higher  $S_8 = 0.799 \pm 0.015$  at the  $2\sigma$  level [8, 9] in the framework of  $\Lambda$ CDM. However, a re-analysis with the combination of DES data [10] and KiDS/Viking [11, 12] established the tension at the  $3\sigma$  level with the value  $S_8 = 0.755^{+0.019}_{-0.021}$  [12]. The tension arises due to a lower matter clustering at scales  $k \approx 0.1 - 1h \text{ Mpc}^{-1}$ , and a reduction in the amplitude of matter fluctuations on those scales can effectively resolve it.

Despite numerous attempts, alternative CDM scenarios such as WDM or mixed dark matter models have

\* [amlan.chakraborty@iiap.res.in](mailto:amlan.chakraborty@iiap.res.in)

† [anirbandas@snu.ac.kr](mailto:anirbandas@snu.ac.kr)

‡ [subinoy@iiap.res.in](mailto:subinoy@iiap.res.in)

§ [sethi@rri.res.in](mailto:sethi@rri.res.in)

failed to resolve the  $S_8$  tension. Adding massive thermal neutrinos, one of the proposed solutions does not alleviate the tension. This is because an increase in  $\Delta N_{\text{eff}}$  can raise  $\sigma_8$  and lower  $\Omega_m$ , which exacerbates the tension [1, 13]. Various approaches have been explored, such as decaying dark matter [14–21] and non-thermal dark matter models [13, 22–26], to address this issue.

In this paper, we investigate the cosmological signatures of a novel scenario of mass-varying DM (MVDM) that is a natural generalization of the extra radiation  $N_{\text{eff}}$  and the WDM models. The realisation of an MVDM scenario has been previously suggested in many particle physics models [27–30]. However, in this work, we refrain from assuming any particular model and assume a phenomenological relation proposed in [31].

Previously, cosmological effects of late formation of massive DM were studied in Refs. [31–34]. Similar phenomenon can also occur in models with late primordial black hole formation [35, 36]. Particularly in Ref. [31], some of the authors showed in a model-independent approach that the Lyman- $\alpha$  data from small scale places strong constraint on the transition redshift  $z_t$ . Here we follow a similar phenomenological approach to model the time-variation of DM mass from zero to a finite value.

We perform a comprehensive Bayesian analysis of this model using the latest cosmic microwave background (CMB) data from Planck and ACT. Our study reveals a lower bound on the transition redshift  $z_t$  ( $\log_{10} z_t > 4.55$ ) and a detection of the final mass of the DM, which is estimated to be 41.7 eV when the Planck [1] and KIDS1000+BOSS+2dfLenS weak lensing data [37] are taken into account. The results indicate that the weak lensing data favors this model. Moreover, the inclusion of weak lensing data significantly reduces the  $S_8$  tension as compared to the case when only Planck data is considered.

The plan of the paper is as follows. In section II, we describe the model and the framework of MVDM, and discuss its cosmological signatures. In section III, we present the method of our Markov Chain Monte Carlo (MCMC) analysis with different datasets, and discuss the results in the section IV. Finally, we conclude in section V.

## II. BACKGROUND DENSITY EVOLUTION AND PERTURBATIONS

This study postulates that Mass-Varying Dark Matter is a fermionic species with a temperature of  $T$ . In this paper, we do not commit to a particular particle physics model for the mass variation of DM. Instead, we adopt the phenomenological relation proposed in Ref. [31]. The essential concept is that DM was massless and relativistic in the early time, and at a transition redshift of  $z_t$ , it underwent an instantaneous transition to become non-relativistic. The form of  $m(z)$  considered in this analysis

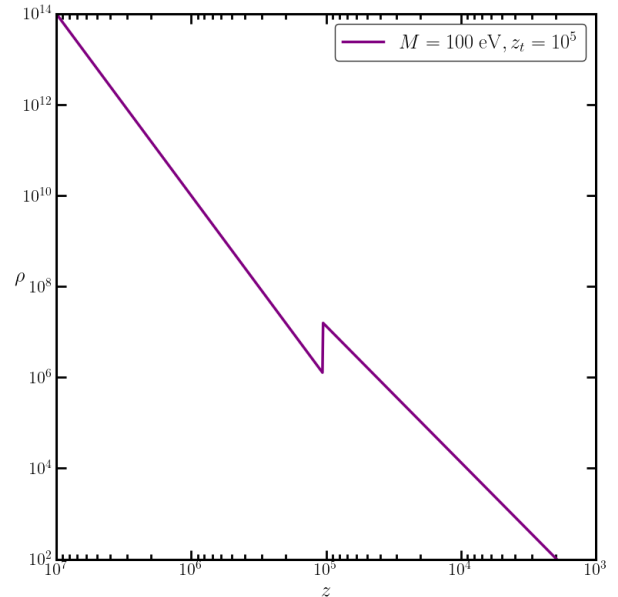


Figure 1. Evolution of background energy density with redshifts is plotted for mass  $M = 100$  eV for a transitional redshift  $z_t = 10^5$ .

is as follows

$$m(z) = \frac{M}{2} \left[ 1 - \tanh \left( \frac{z - z_t}{\Delta z} \right) \right]. \quad (1)$$

Here,  $M$  denotes the final mass of MVDM, whereas the redshift duration of the transition is represented by  $\Delta z$ . We note that, due to our assumption of the instantaneous nature of the transition, the value of  $\Delta z$  is considerably smaller than that of  $z_t$  ( $\Delta z \ll z_t$ ). Consequently, the DM instantaneously loses its relativistic nature, necessitating the ratio of the final mass ( $M$ ) to the transition temperature ( $T_t$ ) to be significantly greater than unity, i.e.,  $M/T_t \gg 1$ .

We take the phase space distribution of MVDM to be Fermi-Dirac, which enables us to calculate the energy density and other higher moments of the distribution. Due to the rapid transition, the energy density exhibits a jump during its evolution at  $z_t$ , which can be expressed as the quantity  $\rho_{\text{MVDM}}^{\text{NR}}(z \rightarrow z_t^+) / \rho_{\text{MVDM}}^{\text{R}}(z \rightarrow z_t^-) = M/T_t$ . This phenomenon is accurately depicted in Figure 1 for a particular value of  $z_t$ . For the remainder of this paper, we have set the MVDM temperature to  $T = T_\gamma/10$  in the relativistic phase as a representative value. The mass of a light, Fermionic dark matter particle can be constrained by Tremaine-Gunn bound [38]. This bound can be cast in terms of the value of initial (fine-grained) phase space distribution function (Ref. [38], Eq.(18.64)). The constraint depends on the ratio  $M/T$ , which means the bounds needs to be scaled by the corresponding factor for our choice of the temperature,  $T$ . We note that the parameter space studied in the paper is consistent with this bound.

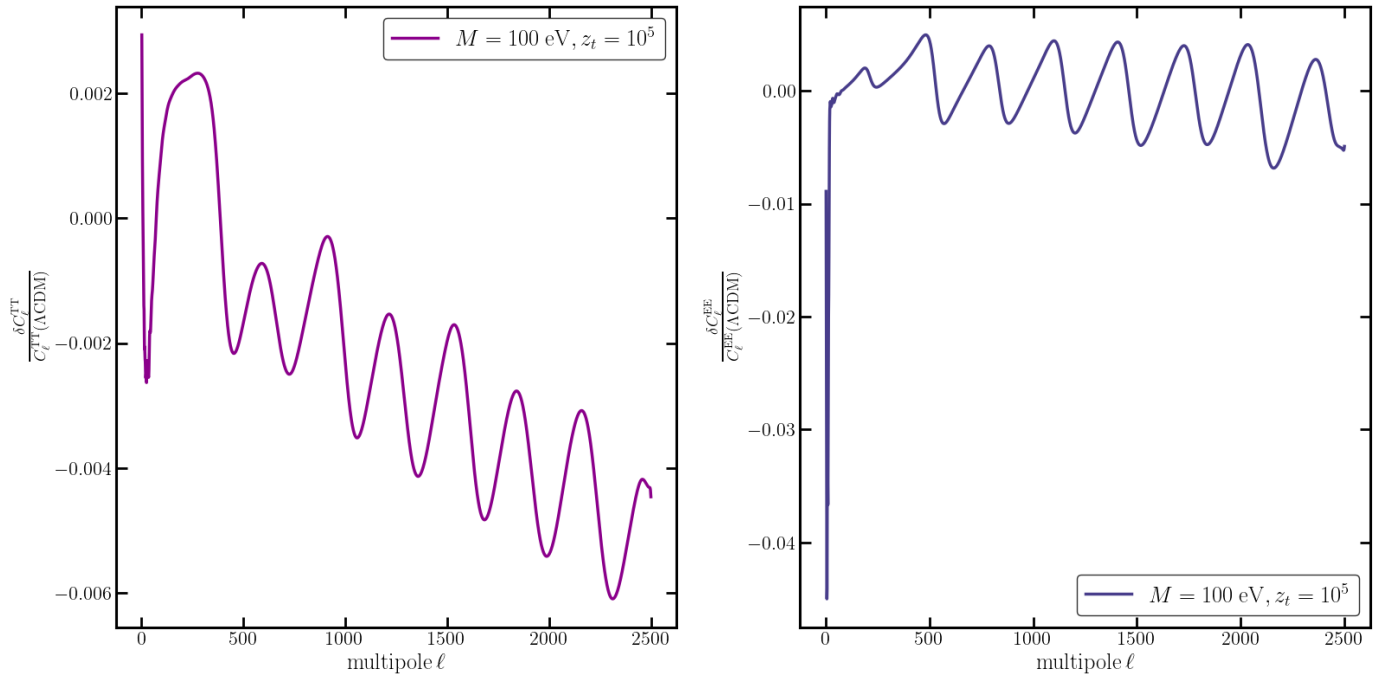


Figure 2. The relative change in the CMB TT and EE power spectra with respect to  $\Lambda\text{CDM}$  is plotted for mass  $M = 100$  eV for a transitional redshift  $z_t = 10^5$ .

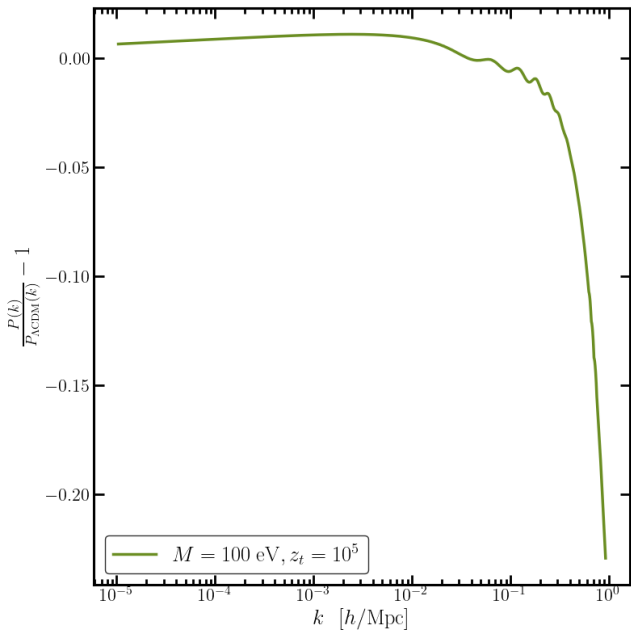


Figure 3. Relative change in matter power spectra with respect to  $\Lambda\text{CDM}$  is plotted for mass  $M = 100$  eV for a transitional redshift  $z_t = 10^5$ .

Because of its relativistic nature before  $z_t$ , MVDM will contribute to the total radiation energy density, thereby affecting the evolution of the universe and leaving an imprint on observables such as the CMB and the matter power spectra. This contribution can be quantified as an

additional relativistic degree of freedom,  $\Delta N_{\text{eff}}$ , given by [31],

$$\Delta N_{\text{eff}} \approx \frac{\rho_{\text{MVDM}}(z=0)}{\rho_{\nu}^{\text{th}}(z=0)} \frac{T_t}{M} \frac{1}{1+z_t} \quad (2)$$

This model shows observable effects at the perturbation level as well. The transition of DM from relativistic to non-relativistic phase introduces a cut-off scale, denoted by  $k_t$ , in our model, which corresponds to the fluctuations that entered the horizon at the transition redshift  $z_t$ . Prior to the transition redshift, DM was relativistic and free streaming, prohibiting the growth of structure for the modes that entered before  $z_t$ . This results in a suppression of power for  $k > k_t$  in the matter power spectra shown in Figure 3. For lower transition redshift, the suppression moves to larger scales, implying the structure is washed away at lower  $k$  modes. Furthermore, the free streaming length is directly proportional to the thermal velocity of DM particles, i.e.,  $v_{th} = \frac{\langle p \rangle}{m}$ . Therefore, the cut-off scale  $k_t$ , which is determined from the free-streaming length during the transition, is also dependent on the final mass of the DM [39–42]. Consequently, we obtain smaller  $k_t$  values for DM with lighter mass. This suppression of power is also reflected in the CMB temperature and polarization anisotropy power spectrum at higher  $\ell$ , as shown in Figure 2.

The presence of free-streaming dark matter (DM) particles during their relativistic phase causes a small but non-zero  $\Delta N_{\text{eff}}$ , which exerts an additional drag on the metric perturbation via gravity during the radiation-

dominated era. This results in an extra phase shift in the acoustic oscillation of the photon-baryon plasma that can be detected in both the cosmic microwave background (CMB) and the matter power spectrum as small wiggles, which can be seen in both Figure 2 & 3.

### III. METHOD

We use the Boltzmann hierarchy for the MVDM model implemented in CLASS in Ref. [31] to compute the CMB anisotropy power spectra and the matter power spectrum [45].

We perform a comprehensive Markov Chain Monte Carlo (MCMC) analysis of the MVDM model using following combinations of cosmological datasets:

- ▶ Planck 2018 measurements of the low- $\ell$  CMB TT, EE, and high- $\ell$  TT, TE, EE power spectra [1].
- ▶ The KIDS1000+BOSS+2dfLenS weak lensing data are analysed in a 'multi-probe' setting, i.e. three sets of two-point statistics are analysed simultaneously to evaluate the likelihood on the parameter  $S_8 = 0.766^{+0.02}_{-0.014}$  [37].
- ▶ ACT data from ACT collaboration, which includes the DR4 data release [43]. We use `actpollite dr4` likelihood code which contains TT measurements ( $600 < \ell < 4126$ ) and TE and EE measurements ( $350 < \ell < 4126$ ). Since it does not have large-scale data, constraining reionization optical depth  $\tau_{\text{reio}}$  is not possible. So a Gaussian prior is also added, centered at  $\tau_{\text{reio}} = 0.06 \pm 0.01$  while analyzing ACT data alone [44].

In this study, we adopt the standard  $\Lambda$ CDM model as our base framework, which comprises of the six parameters:  $\omega_b, \omega_{\text{cdm}}, 100 \times \theta_s, \ln 10^{10} A_s, n_s, \tau_{\text{reio}}$ . To incorporate our MVDM model, we introduce two additional parameters  $\log_{10} z_t, M$  in conjunction with the six aforementioned parameters.

The MCMCs are executed using the MontePython-v3 [46] code implemented with the Metropolis-Hasting algorithm. We utilize our modified CLASS version to interface with the MCMCs. We obtain all the reported  $\chi^2_{\text{min}}$  values using the Python package iMinuit [47]. We use a Choleski decomposition to handle various nuisance parameters [48] better and consider chains to be converged when the Gelman-Rubin convergence criterium  $R - 1 \lesssim 0.01$  [49].

### IV. RESULTS

We performed MCMC runs for both the  $\Lambda$ CDM and MVDM models using the two datasets. We present our results in Fig. 4 and Table I. The  $\chi^2_{\text{min}}$  values per experiment are quoted in the Appendix.

For the Planck-only analysis with the MVDM cosmology, we were able to obtain a bound on the mass  $M > 23 \text{ eV}$  and  $\log_{10} z_t > 4.72$  (obtained at half of the peak posterior value of the respective parameter). Our analysis yields  $S_8(\text{MVDM}) = 0.822^{+0.0236}_{-0.0179}$ , which is to be compared to  $S_8(\Lambda\text{CDM}) = 0.831^{+0.0164}_{-0.0165}$ . MVDM shifts  $S_8$  downward almost by  $\sim 0.5\sigma$ , thus effectively reducing the level of  $S_8$  tension from  $\sim 2.7\sigma$  to  $\sim 2.2\sigma$ . So, MVDM prefers a slightly lower value of  $S_8$ , and the minimum  $\chi^2$  shows a slight improvement compared to the standard  $\Lambda$ CDM model i.e.  $\Delta\chi^2_{\text{min}} = \chi^2_{\text{min}}(\text{MVDM}) - \chi^2_{\text{min}}(\Lambda\text{CDM}) = -1.23$ .

The inclusion of the  $S_8$  prior in our analysis yields significant results. Specifically, we observe a mild detection of dark matter final mass  $M = 41.7^{+7.81}_{-27.5} \text{ eV}$  and a tighter constraint on  $\log_{10} z_t > 4.67$  in the MVDM model. We get  $S_8(\text{MVDM}) = 0.79^{+0.0209}_{-0.0167}$  in this likelihood combination, which can be compared to our baseline  $S_8(\Lambda\text{CDM}) = 0.805^{+0.0126}_{-0.0129}$ . Consequently, the  $\chi^2_{\text{min}}$  in the combined analysis decreases for the MVDM case, with  $\Delta\chi^2_{\text{min}} = \chi^2_{\text{min}}(\text{MVDM}) - \chi^2_{\text{min}}(\Lambda\text{CDM}) = -3.81$ . Further, we note that the overall  $\chi^2_{\text{min}}$  is less impacted by the inclusion of the  $S_8$  prior in the MVDM case (+3.78) as compared to that in the  $\Lambda$ CDM case (+6.36). This finding strongly indicates that the MVDM model is better suited to explain both CMB and weak lensing data compared to  $\Lambda$ CDM. We also report the individual contribution from each dataset in each run for both of the models is reported in Table III in Appendix A.

To gain a deeper understanding of the results obtained from the MCMC analysis, we present residual plots in Figure 5 for the CMB TT, EE power spectra, and the matter power spectra with respect to  $\Lambda$ CDM in the best-fit mass-varying dark matter (MVDM) model obtained when Planck+ $S_8$  data is considered. Notably, the suppression of power at small length scales (i.e., large  $k$  modes and large  $\ell$ 's) is a crucial factor in mitigating the tension.

As mentioned in Section II and [31], this suppression is attributed to the fact that the mass-varying dark matter stays relativistic until the transition redshift  $z_t$ , contributing to the relativistic energy density, which can be quantified through additional degrees of freedom in Equation 2. This effect washes away all perturbations at very small length scales, as evidenced by the matter power spectra residual plot and CMB TT, EE residual plots in Figure 5. Consequently, we observe a reduction in the  $S_8$  value relative to Planck due to the reduction in fluctuation amplitude on scales  $k \approx 0.1 - 1 h \text{ Mpc}^{-1}$  as discussed in the Introduction. The addition of  $S_8$  prior yields a mild preference the mass of MVDM at around 23.87 eV (best-fit value), as shown in Figure 4. These results clearly demonstrate that the KIDS1000+BOSS+2dfLenS weak lensing data favours the MVDM model. It should be noted that the error bars in the angular power spectra from Planck are larger at higher  $\ell$  owing to Planck beam, which makes it difficult to put a stringent bound on the Dark Mat-

Table I. The mean (best-fit)  $\pm 1\sigma$  error of the cosmological parameters in the  $\Lambda$ CDM and MVDM model obtained from the analysis of Planck [1] and Planck+ $S_8$ [37] data. Lower limits are obtained at half of the peak posterior value of the respective parameter.

Model	$\Lambda$ CDM		MVDM	
Parameter	Planck	Planck+ $S_8$	Planck	Planck+ $S_8$
$100\omega_b$	$2.24(2.2334)^{+0.0154}_{-0.0155}$	$2.25(2.2528)^{+0.0145}_{-0.0146}$	$2.24(2.239)^{+0.0153}_{-0.0157}$	$2.25(2.245)^{+0.0152}_{-0.0156}$
$\omega_{\text{dm}}^{\text{a}}$	$0.12(0.1199)^{+0.00141}_{-0.0014}$	$0.118(0.1178)^{+0.00114}_{-0.00118}$	$0.12(0.1208)^{+0.00141}_{-0.00143}$	$0.119(0.12)^{+0.00134}_{-0.00158}$
$100 \times \theta_s$	$1.04(1.04184)^{+0.000304}_{-0.0003}$	$1.04(1.04215)^{+0.000301}_{-0.000294}$	$1.04(1.042)^{+0.000322}_{-0.000353}$	$1.04(1.0419)^{+0.000317}_{-0.000362}$
$n_s$	$0.965(0.96754) \pm 0.00453$	$0.969(0.972)^{+0.00421}_{-0.00422}$	$0.968(0.9655)^{+0.00466}_{-0.00503}$	$0.97(0.965)^{+0.00493}_{-0.00511}$
$\ln 10^{10} A_s$	$3.04(3.0391)^{+0.0156}_{-0.0162}$	$3.04(3.021)^{+0.0159}_{-0.0158}$	$3.05(3.0442)^{+0.0162}_{-0.0173}$	$3.04(3.042)^{+0.0158}_{-0.0171}$
$\tau_{\text{reio}}$	$0.0541(0.0517)^{+0.00763}_{-0.00786}$	$0.0521(0.0507)^{+0.00799}_{-0.00785}$	$0.0546(0.0597)^{+0.00786}_{-0.00847}$	$0.0538(0.05198)^{+0.00758}_{-0.00826}$
$\log_{10} z_t$	—	—	$> 4.72$	$> 4.67$
$M[\text{eV}]$	—	—	$> 23$	$41.7(23.87)^{+7.81}_{-27.5}$
$S_8$	$0.831(0.827)^{+0.0164}_{-0.0165}$	$0.805(0.8114)^{+0.0126}_{-0.0129}$	$0.822(0.821)^{+0.0236}_{-0.0179}$	$0.79(0.776)^{+0.0209}_{-0.0323}$
$\Omega_m$	$0.315(0.3138)^{+0.00852}_{-0.00867}$	$0.303(0.3064)^{+0.00672}_{-0.00712}$	$0.309(0.301)^{+0.00823}_{-0.00884}$	$0.302(0.311)^{+0.00759}_{-0.0095}$
$H_0[\text{Km/s/Mpc}]$	$67.3(67.35)^{+0.602}_{-0.643}$	$68.2(67.88)^{+0.528}_{-0.527}$	$67.9(67.52)^{+0.638}_{-0.636}$	$68.4(67.96)^{+0.695}_{-0.606}$
$\chi_{\text{min}}^2$	2771.78	2778.14	2770.55	2774.33

<sup>a</sup> for  $\Lambda$ CDM model, the 'dm' subscript means the Cold Dark Matter (CDM), and for the MVDM model, it means the mass varying dark matter considered in this paper.

Table II. The mean (best-fit)  $\pm 1\sigma$  error of the cosmological parameters in the  $\Lambda$ CDM and MVDM model obtained from the analysis of ACT [43, 44] and ACT+ $S_8$ [37] data. Lower limits are obtained at half of the peak posterior value of the respective parameter.

Model	$\Lambda$ CDM		MVDM	
Parameter	ACT	ACT+ $S_8$	ACT	ACT+ $S_8$
$100\omega_b$	$2.15(2.1471)^{+0.0308}_{-0.0318}$	$2.16(2.1561)^{+0.0307}_{-0.0314}$	$2.16(2.166) \pm 0.0317$	$2.17(2.1698)^{+0.0304}_{-0.0323}$
$\omega_{\text{dm}}^{\text{a}}$	$0.118(0.1171)^{+0.00373}_{-0.00384}$	$0.114(0.11401)^{+0.00162}_{-0.00177}$	$0.118(0.11839)^{+0.00379}_{-0.00385}$	$0.115(0.1168)^{+0.00179}_{-0.00266}$
$100 \times \theta_s$	$1.04(1.0433)^{+0.000728}_{-0.000708}$	$1.04(1.04385)^{+0.000666}_{-0.000686}$	$1.04(1.0436)^{+0.000723}_{-0.000727}$	$1.04(1.0436)^{+0.000691}_{-0.000698}$
$n_s$	$1.01(1.0092)^{+0.0156}_{-0.0159}$	$1.02(1.0177)^{+0.0142}_{-0.0144}$	$1.01(1.00945)^{+0.0154}_{-0.0164}$	$1.02(1.0131)^{+0.0147}_{-0.0149}$
$\ln 10^{10} A_s$	$3.04(3.04165)^{+0.0224}_{-0.0238}$	$3.03(3.0332)^{+0.0209}_{-0.0223}$	$3.04(3.0421)^{+0.0225}_{-0.0239}$	$3.03(3.029)^{+0.0209}_{-0.0232}$
$\tau_{\text{reio}}$	$0.0604(0.06058)^{+0.00927}_{-0.01}$	$0.0601(0.06145)^{+0.00897}_{-0.0102}$	$0.0606(0.05936)^{+0.00922}_{-0.0103}$	$0.0604(0.05645)^{+0.00914}_{-0.0102}$
$\log_{10} z_t$	—	—	$> 5.1$	$> 5.2$
$M[\text{eV}]$	—	—	$> 27$	$51.2(25.31)^{+16}_{-33.5}$
$S_8$	$0.826(0.8169)^{+0.0419}_{-0.044}$	$0.777(0.78)^{+0.016}_{-0.0183}$	$0.817(0.8159)^{+0.0452}_{-0.046}$	$0.777(0.7711)^{+0.0159}_{-0.0183}$
$\Omega_m$	$0.303(0.2986)^{+0.0202}_{-0.023}$	$0.279(0.2822)^{+0.00842}_{-0.00955}$	$0.3(0.2998)^{+0.0203}_{-0.0226}$	$0.283(0.2913)^{+0.00916}_{-0.0143}$
$H_0[\text{Km/s/Mpc}]$	$67.9(68.11)^{+1.51}_{-1.55}$	$69.6(69.384)^{+0.736}_{-0.699}$	$68.4(68.339)^{+1.51}_{-1.58}$	$69.6(68.95)^{+1.06}_{-0.768}$
$\chi_{\text{min}}^2$	280.0495	281.8939	275.7832	276.7859

<sup>a</sup> for  $\Lambda$ CDM model, the 'dm' subscript means the Cold Dark Matter (CDM), and for the MVDM model, it means the mass varying dark matter considered in this paper.

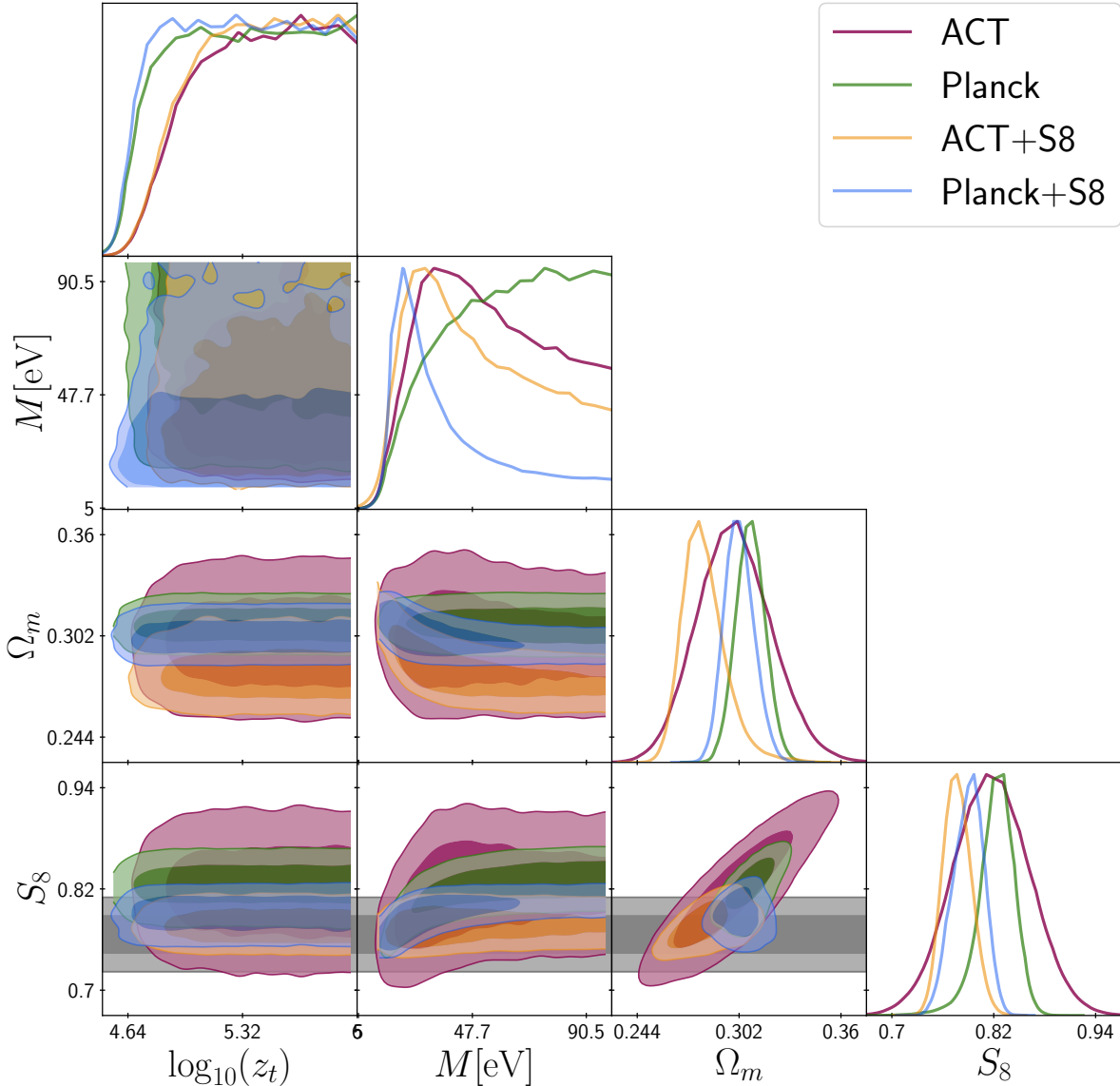


Figure 4. Reconstructed 2D and 1D marginalized posterior distributions of  $\log_{10} z_t, M(\text{eV}), \Omega_m, S_8$  with 68% and 95% confidence level. The weak lensing measurement of  $S_8$  is shown as gray bands (68% and 95%).

ter mass. This is because significant deviations from the standard  $\Lambda\text{CDM}$  paradigm occur only at small length scales, as is evident from the matter power spectra residual plot.

To address this issue, we have also done our MCMC analysis using ACT data, which has better angular resolution than Planck and has measured the CMB power spectra up to  $\ell \simeq 4000$ . The results are also included in Figure 4 and in Table II, where it is clear that the ACT data does a slightly better job in constraining the mass of dark matter and lowering the  $S_8$  value than Planck. ACT data provides a lower limit on the mass  $M > 27 \text{ eV}$  and  $\log_{10} z_t > 5.1$  (obtained at half of the peak posterior values of the respective parameters). Our analysis also shows  $S_8(\text{MVDM}) = 0.817^{+0.0452}_{-0.046}$ , compared

to  $S_8(\Lambda\text{CDM}) = 0.826^{+0.0419}_{-0.044}$  where MVDM lowers  $S_8$  by  $0.2\sigma$ . We also observe an improvement in minimum  $\chi^2$  over  $\Lambda\text{CDM}$ , i.e.  $\Delta\chi^2_{\min} = \chi^2_{\min}(\text{MVDM}) - \chi^2_{\min}(\Lambda\text{CDM}) = -4.2663$ .

In addition to the  $S_8$  value, we find a tighter lower bound on  $\log_{10} z_t > 5.2$ . It also tightens the constraint on the dark matter mass  $M = 51.2(25.31)^{+16}_{-33.5} \text{ eV}$ , compared to previous ACT analysis, but this constraint is much weaker than that of Planck+S8. We find  $S_8(\text{MVDM}) = 0.777^{+0.0159}_{-0.0183}$  in comparison with  $S_8(\Lambda\text{CDM}) = 0.777^{+0.016}_{-0.0183}$ , showing no significant change in the  $S_8$  values in both of the model corresponding to the same dataset except for their best-fit values, given in Table II. However, the addition of prior reduces the  $S_8$  tension significantly compared to all the previous analy-

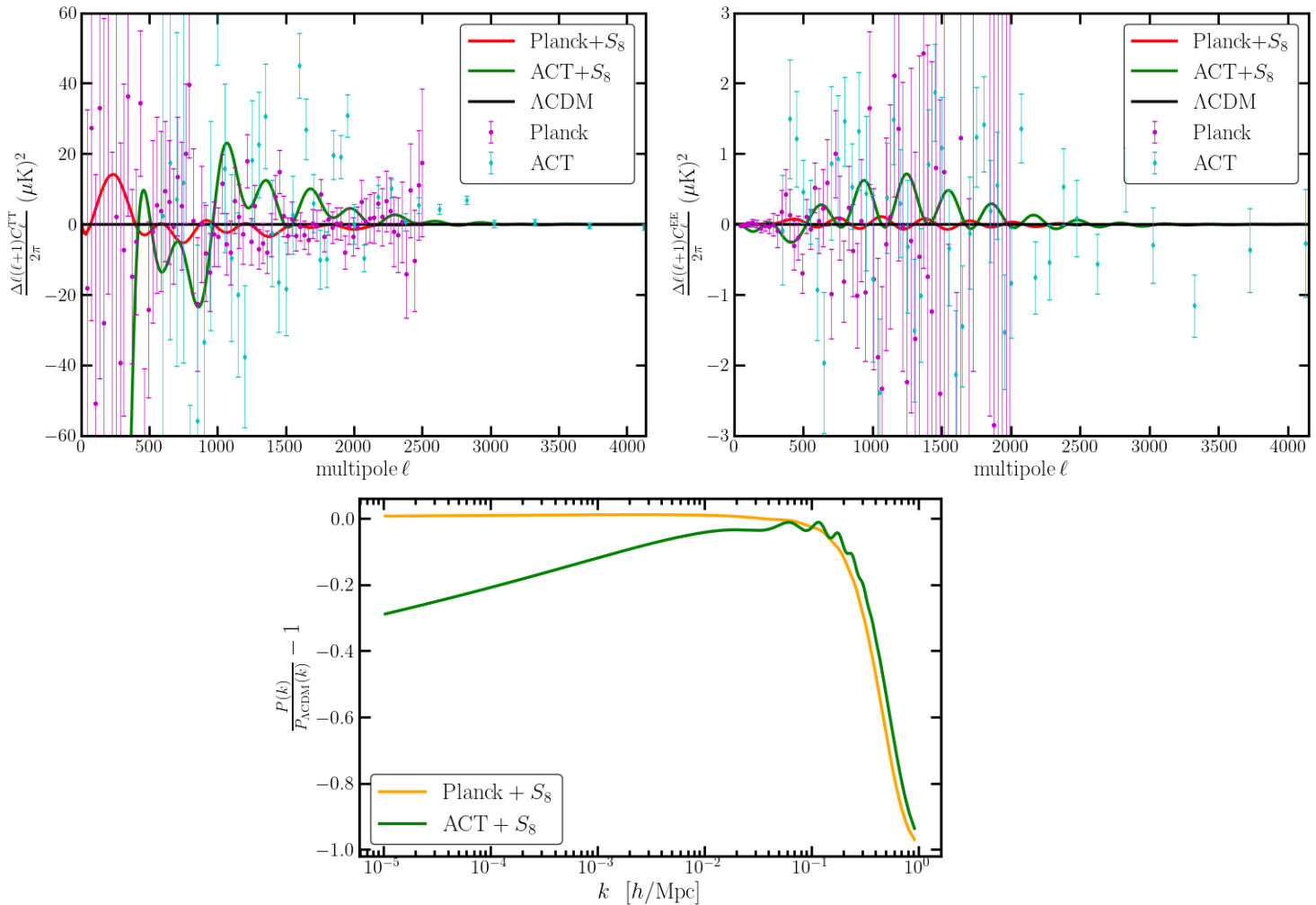


Figure 5. Residuals of the CMB TT, EE (top panel) and matter (bottom panel) power spectra with respect to  $\Lambda$ CDM in the best fit MVDM model for Planck+ $S_8$  and ACT+ $S_8$  data set.

ses considered in this work. To get a better understanding, in Appendix B, we have also plotted the contour plot between  $S_8$  and  $\Omega_m$  for each dataset in Figure 6 and compared both MVDM and  $\Lambda$ CDM models for each of them.  $\chi_{min}^2$  in the combined analysis decreases for the MVDM case, with  $\Delta\chi_{min}^2 = \chi_{min}^2(MVDM) - \chi_{min}^2(\Lambda CDM) = -5.108$ . The individual contribution from each dataset in each run for both models is reported in Table IV in Appendix A.

Future CMB experiments such as CMB-S4 will improve both coverage and sensitivity at small angular scales [50, 51] and therefore holds immense potential for the determination of the nature of Cold Dark Matter.

Furthermore, our MCMC analysis yields the lowest lower bound on  $\log_{10} z_t > 4.55$  out of all the various combinations of datasets, which is expected, given that the model imposes no minimum duration for the dark matter to remain relativistic. It is worth noting that the lower bound must be higher than the redshift of recombination to avoid significant impacts on the CMB power

spectra. We have also performed an MCMC analysis by considering all of the datasets into account (i.e. both Planck+ACT and Planck+ACT+ $S_8$ ). However, no significant change in the result was observed.

## V. CONCLUSIONS

In this study, we explored the model of a mass-varying dark matter, where it transitions from a relativistic to a nonrelativistic phase in the early Universe, and derived constraints using cosmological observation data. We assumed a phenomenological relation of dark matter mass as a function of redshift without invoking any specific particle physics model. We focused only on fast transitions in this work. The large free streaming velocity in the relativistic phase of DM at early time washes out the structures at small scales and manifests its effect in resolving the long-standing  $S_8$  tension between the amplitude of matter fluctuations determined from local [8–

12, 37] and high redshift probes [1], as depicted in Figure 4. The MCMC analysis reveals a slight reduction in  $S_8$  when the model is confronted with only Planck data. However, the inclusion of KIDS1000+BOSS+2dfLenS weak lensing data significantly reduces the  $S_8$ . Furthermore, the model puts a lower bound on the transition redshift and predicts the final mass of the dark matter to be 23.87 eV, with weak-lensing data supporting the model. Similar  $\sim$  eV order warm dark matter mass has also been predicted in other models [52].

The CMB observations obtained from Planck have been used to measure the angular power spectrum. However, the Planck data has large uncertainties at high multipoles, as discussed in the previous section. The MVDM model displays its unique features at high multipoles, which are associated with small length scales. As such, the use of Planck data alone hinders the detection and proper constraint of the DM mass. Since ACT data provides those measurements at higher multipoles with comparatively better precision, our MCMC analysis revealed a better constraining of mass  $M$  compared to Planck and including KIDS1000+BOSS+2dfLenS weak lensing data even further reduces the  $S_8$ , thus resolving the  $S_8$  tension.

Future experiments, such as CMB-S4 [50, 51], are expected to achieve higher precision measurements at high multipoles, specifically for goals related to de-lensing the inflationary B-modes, constraining  $N_{\text{eff}}$  and  $\Sigma m_\nu$ , among others. Such experiments are expected to provide insight into the detailed small-scale physics of the universe, which could aid in the detection and proper constraint of

the DM mass  $M$  of our model. In this regard, a Fisher forecast can also be conducted in the future. Another way to probe such a model is through CMB spectral distortion as shown in [53], which might also be detected in the above-mentioned future experiments.

As previously mentioned, we did not invoke any specific particle physics model to explain the mass variation of dark matter. However, considering a particular particle physics model could potentially introduce additional model-dependent effects beyond those reported in this work. The residual plots of CMB power spectra and matter power spectra, as shown in Figure 5 and referenced in [31], exhibit oscillatory structures resulting from the additional drag force exerted by the relativistic DM, leading to a phase shift in the baryon acoustic oscillation (BAO). A similar phenomenon could occur in the dark sector too. This model could also be employed to constraint the dark acoustic oscillation (DAO) [54, 55]. Additionally, the present model could potentially be explored in light of Lyman- $\alpha$  forest flux power spectrum data in line with recent works [24, 56–62]. However, this is currently outside the scope of this paper. Nevertheless, it remains a goal for future research to investigate the applicability of this model to the aforementioned data.

#### ACKNOWLEDGMENTS

AC thanks Ranjan Laha for the useful discussions regarding this work as well as some of the future works mentioned above. AD was supported by Grant Korea NRF-2019R1C1C1010050. SD acknowledges the DST-SERB Government of India grant CRG/2019/006147 for supporting the project

- 
- [1] N. Aghanim *et al.* (Planck Collaboration), *A&A* **641**, A6 (2020).
- [2] P. Salucci, *The Astronomy and Astrophysics Review* **27**, 2 (2019).
- [3] M. Viel, G. D. Becker, J. S. Bolton, and M. G. Haehnelt, *Phys. Rev. D* **88**, 043502 (2013).
- [4] E. B. Holm, T. Tram, and S. Hannestad, *Journal of Cosmology and Astroparticle Physics* **2022** (08), 044.
- [5] N. Blinov, C. Keith, and D. Hooper, *Journal of Cosmology and Astroparticle Physics* **2020** (06), 005.
- [6] S. Alexander, H. Bernardo, and M. W. Toomey, *Journal of Cosmology and Astroparticle Physics* **2023** (03), 037.
- [7] E. Abdalla *et al.*, *JHEAp* **34**, 49 (2022), arXiv:2203.06142 [astro-ph.CO].
- [8] C. Heymans *et al.*, *Monthly Notices of the Royal Astronomical Society* **432**, 2433 (2013), <https://academic.oup.com/mnras/article-pdf/432/3/2433/12627095/stt601.pdf>.
- [9] N. MacCrann, J. Zuntz, S. Bridle, B. Jain, and M. R. Becker, *Monthly Notices of the Royal Astronomical Society* **451**, 2877 (2015), <https://academic.oup.com/mnras/article-pdf/451/3/2877/4025570/stv1154.pdf>.
- [10] T. M. C. Abbott *et al.* (Dark Energy Survey Collaboration 1), *Phys. Rev. D* **98**, 043526 (2018).
- [11] H. Hildebrandt *et al.*, *A&A* **633**, A69 (2020).
- [12] S. Joudaki *et al.*, *A&A* **638**, L1 (2020).
- [13] V. Poulin, K. K. Boddy, S. Bird, and M. Kamionkowski, *Phys. Rev. D* **97**, 123504 (2018).
- [14] K. Enqvist, S. Nadathur, T. Sekiguchi, and T. Takahashi, *Journal of Cosmology and Astroparticle Physics* **2015** (09), 067.
- [15] V. Poulin, P. D. Serpico, and J. Lesgourgues, *Journal of Cosmology and Astroparticle Physics* **2016** (08), 036.
- [16] K. Vattis, S. M. Koushiappas, and A. Loeb, *Phys. Rev. D* **99**, 121302 (2019).
- [17] B. S. Haridasu and M. Viel, *Monthly Notices of the Royal Astronomical Society* **497**, 1757 (2020), <https://academic.oup.com/mnras/article-pdf/497/2/1757/33562858/staa1991.pdf>.
- [18] S. J. Clark, K. Vattis, and S. M. Koushiappas, *Phys. Rev. D* **103**, 043014 (2021).
- [19] K. L. Pandey, T. Karwal, and S. Das, *Journal of Cosmology and Astroparticle Physics* **2020** (07), 026.
- [20] G. F. Abellán, R. Murgia, V. Poulin, and J. Lavalley, *Phys. Rev. D* **105**, 063525 (2022).
- [21] G. F. Abellán, R. Murgia, and V. Poulin, *Phys. Rev. D* **104**, 123533 (2021).



- [22] C. D. Kreisch, F.-Y. Cyr-Racine, and O. Doré, *Phys. Rev. D* **101**, 123505 (2020).
- [23] R. Murgia, S. Gariazzo, and N. Fornengo, *Journal of Cosmology and Astroparticle Physics* **2016** (04), 014.
- [24] M. Archidiacono, D. C. Hooper, R. Murgia, S. Bohr, J. Lesgourgues, and M. Viel, *Journal of Cosmology and Astroparticle Physics* **2019** (10), 055.
- [25] N. Becker, D. C. Hooper, F. Kahlhoefer, J. Lesgourgues, and N. Schöneberg, *Journal of Cosmology and Astroparticle Physics* **2021** (02), 019.
- [26] S. Kumar and R. C. Nunes, *Phys. Rev. D* **94**, 123511 (2016).
- [27] S. Agarwal, P. S. Corasaniti, S. Das, and Y. Rasera, *Phys. Rev. D* **92**, 063502 (2015), [arXiv:1412.1103](https://arxiv.org/abs/1412.1103) [astro-ph.CO].
- [28] S. Das and N. Weiner, *Phys. Rev. D* **84**, 123511 (2011), [arXiv:astro-ph/0611353](https://arxiv.org/abs/astro-ph/0611353).
- [29] P. K. Chanda and S. Das, *Phys. Rev. D* **95**, 083008 (2017), [arXiv:1702.01882](https://arxiv.org/abs/1702.01882) [gr-qc].
- [30] V. Ganesan, A. Chakraborty, T. Ray, S. Das, and A. Banerjee, (2024), [arXiv:2403.14247](https://arxiv.org/abs/2403.14247) [astro-ph.CO].
- [31] A. Das, S. Das, and S. K. Sethi, *Phys. Rev. D* **108**, 083501 (2023), [arXiv:2303.17947](https://arxiv.org/abs/2303.17947) [astro-ph.CO].
- [32] A. Sarkar, S. Das, and S. K. Sethi, *JCAP* **03**, 004, [arXiv:1410.7129](https://arxiv.org/abs/1410.7129) [astro-ph.CO].
- [33] A. Das, B. Dasgupta, and R. Khatri, *JCAP* **04**, 018, [arXiv:1811.00028](https://arxiv.org/abs/1811.00028) [astro-ph.CO].
- [34] S. Das and E. O. Nadler, *Phys. Rev. D* **103**, 043517 (2021).
- [35] S. Bhattacharya, A. Das, and K. Dutta, *JCAP* **10**, 071, [arXiv:2101.02234](https://arxiv.org/abs/2101.02234) [astro-ph.CO].
- [36] A. Chakraborty, P. K. Chanda, K. L. Pandey, and S. Das, *The Astrophysical Journal* **932**, 119 (2022).
- [37] C. Heymans *et al.*, *A&A* **646**, A140 (2021).
- [38] P. J. E. Peebles, *Principles of Physical Cosmology* (Princeton University Press, 1993).
- [39] W. Hu, D. J. Eisenstein, and M. Tegmark, *Phys. Rev. Lett.* **80**, 5255 (1998), [arXiv:astro-ph/9712057](https://arxiv.org/abs/astro-ph/9712057).
- [40] J. Lesgourgues and S. Pastor, *Phys. Rept.* **429**, 307 (2006), [arXiv:astro-ph/0603494](https://arxiv.org/abs/astro-ph/0603494).
- [41] M. Viel, G. D. Becker, J. S. Bolton, and M. G. Haehnelt, *Phys. Rev. D* **88**, 043502 (2013), [arXiv:1306.2314](https://arxiv.org/abs/1306.2314) [astro-ph.CO].
- [42] K. N. Abazajian *et al.* (Topical Conveners: K.N. Abazajian, J.E. Carlstrom, A.T. Lee), *Astropart. Phys.* **63**, 66 (2015), [arXiv:1309.5383](https://arxiv.org/abs/1309.5383) [astro-ph.CO].
- [43] S. Aiola *et al.*, *Journal of Cosmology and Astroparticle Physics* **2020** (12), 047.
- [44] T. Louis *et al.*, *Journal of Cosmology and Astroparticle Physics* **2017** (06), 031.
- [45] J. Lesgourgues, The cosmic linear anisotropy solving system (class) i: Overview (2011), [arXiv:1104.2932](https://arxiv.org/abs/1104.2932) [astro-ph.IM].
- [46] T. Brinckmann and J. Lesgourgues, Montepython 3: boosted mcmc sampler and other features (2018), [arXiv:1804.07261](https://arxiv.org/abs/1804.07261) [astro-ph.CO].
- [47] F. James and M. Roos, *Computer Physics Communications* **10**, 343 (1975).
- [48] A. Lewis, A. Challinor, and A. Lasenby, *The Astrophysical Journal* **538**, 473 (2000).
- [49] A. Gelman and D. B. Rubin, *Statistical Science* **7**, 457 (1992).
- [50] K. N. Abazajian *et al.*, Cmb-s4 science book, first edition (2016), [arXiv:1610.02743](https://arxiv.org/abs/1610.02743) [astro-ph.CO].
- [51] K. Abazajian *et al.*, Snowmass 2021 cmb-s4 white paper (2022), [arXiv:2203.08024](https://arxiv.org/abs/2203.08024) [astro-ph.CO].
- [52] K. K. Rogers and V. Poulin, (2023), [arXiv:2311.16377](https://arxiv.org/abs/2311.16377) [astro-ph.CO].
- [53] A. Sarkar, S. K. Sethi, and S. Das, *Journal of Cosmology and Astroparticle Physics* **2017** (07), 012.
- [54] T. Schaeffer and A. Schneider, *Monthly Notices of the Royal Astronomical Society* **504**, 3773 (2021), <https://academic.oup.com/mnras/article-pdf/504/3/3773/37896468/stab1116.pdf>.
- [55] P. Parashari and R. Laha, *Monthly Notices of the Royal Astronomical Society: Letters* **526**, L63 (2023), <https://academic.oup.com/mnrasl/article-pdf/526/1/L63/54609777/slad107.pdf>.
- [56] C. Miller, A. L. Erickcek, and R. Murgia, *Phys. Rev. D* **100**, 123520 (2019).
- [57] M.-Y. Wang, R. A. C. Croft, A. H. G. Peter, A. R. Zentner, and C. W. Purcell, *Phys. Rev. D* **88**, 123515 (2013).
- [58] R. Murgia, A. Merle, M. Viel, M. Totzauer, and A. Schneider, *Journal of Cosmology and Astroparticle Physics* **2017** (11), 046.
- [59] J. Baur, N. Palanque-Desabrouille, C. Yèche, A. Boryarsky, O. Ruchayskiy, Éric Armengaud, and J. Lesgourgues, *Journal of Cosmology and Astroparticle Physics* **2017** (12), 013.
- [60] R. Murgia, V. Iršič, and M. Viel, *Phys. Rev. D* **98**, 083540 (2018).
- [61] N. Palanque-Desabrouille, C. Yèche, N. Schöneberg, J. Lesgourgues, M. Walther, S. Chabanier, and E. Armengaud, *Journal of Cosmology and Astroparticle Physics* **2020** (04), 038.
- [62] W. Enzi, R. Murgia, O. Newton, S. Vegetti, C. Frenk, M. Viel, M. Cautun, C. D. Fassnacht, M. Auger, G. Despali, J. McKean, L. V. E. Koopmans, and M. Lovell, *Monthly Notices of the Royal Astronomical Society* **506**, 5848 (2021), <https://academic.oup.com/mnras/article-pdf/506/4/5848/39729079/stab1960.pdf>.

## Appendix A: $\chi^2_{min}$ Per Experiment

## Appendix B: $S_8$ with $\Omega_m$ plots for different dataset and models

Table III. Best-fit  $\chi^2_{\min}$  per experiment (and total) for both the model

Experiment	$\Lambda$ CDM		MVDM	
Planck high- $\ell$ TT,TE,EE	2353.36	2358.06	2350.87	2353.6
Planck low- $\ell$ EE	395.75	395.8	396.15	395.84
Planck low- $\ell$ TT	22.67	21.9	23	23.6
KiDS/BOSS/2dFGS	–	2.38	–	1.29
Total	2771.78	2778.14	2770.55	2774.33

Table IV. Best-fit  $\chi^2_{\min}$  per experiment (and total) for both the model

Experiment	$\Lambda$ CDM		MVDM	
ACTPol lite DR4	280.0462	281.1964	275.7791	276.5869
Tau prior	0.0033	395.8	0.0041	0.1261
KiDS/BOSS/2dFGS	–	0.6766	–	0.0729
Total	280.0495	281.8939	275.7832	276.7859

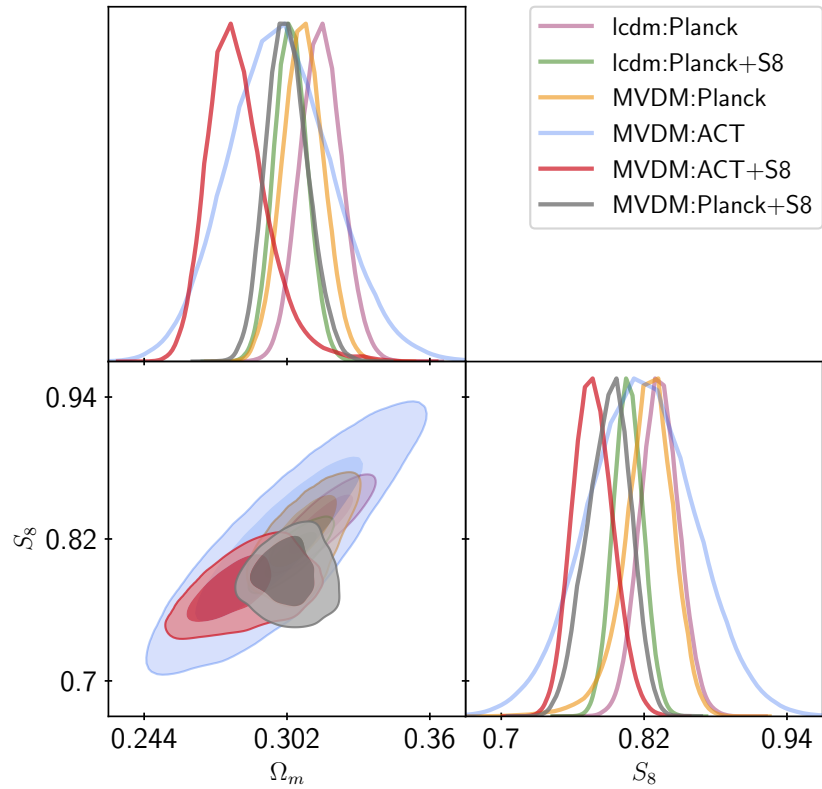


Figure 6. Reconstructed 2D marginalized posterior distributions of  $\Omega_m$  and  $S_8$  with 68% and 95% confidence level.